Nb_2O_5 as a radical modulator during oxidative dehydrogenation and as a Lewis acid promoter in CO_2 assisted dehydrogenation of octane over confined 2D engineered $NiO\text{-}Nb_2O_5\text{-}Al_2O_3$

Majid D. Farahani,[a] Mohamed I. Fadlalla,[b,c] Itegbeyogene P. Ezekiel,[a] Nadir S. E. Osman,[a] Thomas Moyo,[a] Michael Claeys[b,c] and Holger B. Friedrich[a] *

a. School of Chemistry and Physics, University of KwaZulu-Natal, Durban 4000, South Africa
b. Catalysis Institute, Department of Chemical Engineering, University of Cape Town, Rondebosch 7701, South Africa
c. c*change (DST-NRF Center of Excellence in Catalysis)
Email: friedric@ukzn.ac.za

Supporting information

Section S1. EXPERIMENTAL

Section S1.1. Materials

$Ni(NO_3)_2.6H_2O$ (ACS reagent grade), $Al(NO_3)_3.9H_2O$ (ACS reagent grade) and $C_4H_4NNbO_9.xH_2O$ (99.99%) were purchased from Sigma-Aldrich and used as received. An ammonia solution (25%) (Merck) was used to adjust the pH during the synthesis. De-ionized water was used for all steps of the synthesis. For catalytic testing, synthetic air (UHP) and nitrogen (UHP) were produced in-house using Peak Scientific generators and *n*-octane with the assay of >98% was purchased from Alfa Aesar. Argon, carbon dioxide, helium, hydrogen, propane (instrumental grade) and mixed gases such as 10% H_2/N_2, 5% H_2/Ar, 10% O_2/He and 5% NH_3/He cylinders (instrumental grade) were purchased from Afrox and used for different analyses.

Section S1.2. Glycol-thermal synthesis of 25% ($NiO\text{-}Nb_2O_5$)/Al_2O_3

The required amounts of Ni, Nb and Al salts were weighed and dissolved in 500 ml water under constant stirring. Then, the pH of the solution was adjusted to 9 via the addition of ammonia solution which resulted in the formation of a precipitate. The change in the pH of the solution was monitored using pH paper. The solution was stirred (500 rpm) for 15 minutes to ensure that the precipitation was complete. Complete precipitation was achieved since the targeted compositions of each catalyst were achieved according to ICP results. The precipitate was filtered off under vacuum and washed three times using water. The wet precipitate was transferred from the Buchner funnel to a Parr reactor vessel, followed

by addition of 200 ml of ethene glycol. Then, the temperature was set at 200 °C and a stirrer rotation speed of 300 rpm was set. The reaction was carried out overnight and the maximum self-generated pressure was between 130-150 psi (depending on the ratio between the used precursors). Thereafter, the formed thick gel was transferred to a Buchner funnel and washed with water until a neutral pH was achieved, to remove any unreacted ethene glycol. The thick gel was left under an IR lamp (power = 200 W) overnight. Finally, the formed hard solid was crushed using a mortar and pestle and calcined under flow of air at 450 °C for six hours with heating rate of 2 °/min. The final catalysts had a 25 wt.% total loading for different ratios between NiO and Nb_2O_5, whereas 75 wt.% was fixed for alumina. The ratios between wt.% loadings of NiO : Nb_2O_5 were varied in the order of 1:0, 2:1, 1:2 and 0:1, which are labelled in this article as NiAl, 2Ni1NbAl, 1Ni2NbAl and NbAl, respectively.

Section S1.3. Catalytic testing

Section S1.3.1. Oxidative dehydrogenation and dehydrogenation of n-octane and propane

The catalytic testing was performed in a continuous flow fixed bed reactor (in vertical flow mode). A stainless-steel tube with the 10 mm ID and 200 mm length was used as a reactor tube, while the catalysts particles were loaded in the isothermal zone. To eliminate the occurrence of homogenous gas phase reaction, the voids were filled with carborundum (744 μm, Polychem). 0.4 ml (~0.3 g) of fresh catalyst with particle size of 300-600 μm was mixed with the same volume of carborundum in the catalyst bed. The reactions were carried out in the temperature range of 360-600 °C. Nitrogen and air flows were controlled using Bronkhorst mass flow controllers, while the CO_2 flow was controlled using a red-y Vögtlin mass flow controller). *n*-octane was introduced into the reaction via a series II HPLC pump through preheated (140 °C) lines. Propane was feed into the reaction via a red-y Vögtlin mass flow controller. To maintain the GHSV and vary the C:O ratio, the ratio between the flows of air or CO_2 and nitrogen were adjusted. Offline injections were done in three GCs with the following specifications. Hydrocarbon were analysed using a Shimadzu 2121 GC with FID detector and PONA capillary column using H_2 and N_2 as the carrier gases. H_2, CO and CO_2 were analysed using a PerkinElmer Clarus 400 GC equipped with a TCD detector and a Carboxen PLOT 1010 column with argon as a carrier gas.

Unreacted oxygen was quantified using a PerkinElmer Clarus 500 GC equipped with a TCD and PLOT 5A with helium as a carrier gas.

Table S1. A summary of the reaction conditions that were used in this study. The catalyst bed volume is fixed at 0.4 mL.

Conditions	Feed (mL/min)	Additive (mL/min)	N_2 flow (ml/min)
ODH of *n*-octane (C:O = **8:4**, GHSV = 16 000 h^{-1} and concentration of *n*-octane in the feed = 7%	*n*-octane[a] (0.05)	Air (71.7)	28.0
ODH of *n*-octane (C:O = **8:3**, GHSV = 16 000 h^{-1} and concentration of *n*-octane in the feed = 7%	*n*-octane[a] (0.05)	Air (53.8)	45.5
ODH of *n*-octane (C:O = **8:2**, GHSV = 16 000 h^{-1} and concentration of *n*-octane in the feed = 7%	*n*-octane[a] (0.05)	Air (35.8)	63.3
ODH of *n*-octane (C:O = **8:1**, GHSV = 16 000 h^{-1} and concentration of *n*-octane in the feed = 7%	*n*-octane[a] (0.05)	Air (17.9)	81.3
ODH of propane (C:O = 3:1.5, GHSV = 16000 h^{-1} and concentration of propane in the feed = 19%)	propane[b] (20.1)	Air (71.8)	15.3
DH of *n*-octane (GHSV = 13 000 h^{-1} and concentration of *n*-octane in the feed = 12%)	*n*-octane[a] (0.07)	-	77.3
CO_2-DH of *n*-octane (CO_2/*n*-octane molar ratio= 5, GHSV = 13000 h^{-1} and concentration of *n*-octane in the feed = 12%)	*n*-octane[a] (0.07)	CO_2 (52.7)	24.6

a. Liquid flow; This feed was introduced to the reactor (preheated lines) in liquid form using a HPLC pump.

b. Gas flow; This feed was introduced to the reactor in gas form using a mass flow controller.

Section S1.3.2. Reverse water gas shift reaction using CO_2 in hydrogen lean regime

The reverse water gas shift (RWGS) reaction was carried out in a fixed bed reactor, where the catalyst was placed in the isothermal zone and the reactor voids were filled with SiC for heat transfer and heating of reactants. The reactants (i.e. H_2, CO_2 and Ar) flows were controlled via Brooks flow controllers. The reactants and products were analysed by a Varian micro gas chromatograph (CP-4900) equipped with Thermal Conductivity Detectors (μGC) and three separate GC channels: a 20 m M5A, a 10 m PPQ and a 10 m M5A, for the analysis of Ar/CO, CO_2 and H_2 respectively. Reactant ratios and space velocity were set to be similar to the CO_2-ODH reaction.

Section S1.4. Physicochemical characterization

A powder X-Ray diffractometer (Bruker D8 Advance) equipped with a copper radiation source (λ = 1.5406 nm) was used to analyse the catalyst phase(s) composition of the prepared materials as well as the used catalysts obtained from the CO_2-DH. A Bruker D8 advanced XRD instrument equipped with a Co source ($K_{\alpha 1}$ = 1.78897 nm), a Ni filter and a Lynxeye XE detector was used to study the structure of the used catalysts obtained from the RWGS reaction. The redox properties of the catalysts were investigated using an *in situ* XRD Anton Paar XRK 900 reaction chamber in a Bruker D8 Advance equipped with a copper radiation source (λ = 1.5406 nm). The reducing environment was provided using 10% H_2/N_2, and the oxidation cycle was done using synthetic air, while the flow rate was set to 30 mL/min. TPROR (temperature programmed reduction-oxidation-reduction) was carried out in a Micromeritics 2920 Autochem II analyser equipped with a TCD detector. In this analysis 30 mL/min of 5% H_2/Ar (reduction cycles) and 5% O_2/He or pure CO_2 (depending on the experiment for the oxidation cycle) were flowed, whilst the temperature was changed in the range of 80 °C - 800 °C (heating rate = 10 degree/min) with the ROR sequence over the same sample. A Micromeritics 2920 Autochem II analyser equipped with a TCD detector was also utilized for NH_3-TPD (temperature programmed desorption) analysis to establish the surface acidity of these catalysts. During NH_3-TPD, the sample was dosed with 5% NH_3/He (flow = 30 mL/min) for two hours, then, the physiosorbed ammonia was removed by passing He over the sample for 2 hours at 80 °C, where the TCD signal becomes stable. Afterwards, the sample was heated from 80 °C to 800 °C (heating rate = 10 degree/min) under a flow of He (30 mL/min), while the desorbed NH_3 was measured. X-ray photoelectron spectroscopy measurements were done to establish the surface compositions of these catalysts, using a K-Alpha XPS fabricated with a built-in a monochromatic small-spot X- ray source via an aluminium anode AlK_α ($h\nu$ = 1486.6 eV). The background pressure was regulated to be $4.9E^{-8}$ bar or $4.0E^{-7}$ bar of argon during measurement to avoid sample charging. Binding energies were referenced to the sample stage, which contains built in calibration standards of copper, silver, and gold. The bulk compositions of synthesised composites were confirmed with Inductively Coupled Plasma-Optical Emission Spectroscopy using a PerkinElmer Precisely Optima 5300DV, after the sample was digested in H_2SO_4

(98%, Merck). Raman spectra of the used catalysts from CO_2-DH were obtained using a Renishaw inVia Raman microscope at λ = 514nm, 50% laser power and 10 seconds of exposure time. Nitrogen physisorption measurements were done using a Micromeritics Tristar II (T = -196 ºC). Samples were degassed under flow of N_2 at 200 °C with a Micromeritics flow prep 060 overnight prior to each BET analysis. The catalyst morphology was viewed using a Zeiss Ultra plus Scanning Electron Microscope (SEM). The bulk structures of the catalysts were viewed using a Jeol JEM-2100, while a High Resolution-Transmission Electron Microscope (HR-TEM [Jeol JEM-2100]) was used (in STEM mode) to determine the elemental distribution (mapping). The IR spectra of the used catalysts were obtained using a Perkin-Elmer ATR (attenuated total reflectance) spectrometer. The mass/extent of carbon deposition on the fresh and used catalysts during the RWGS reaction and CO_2-DH were analysed by a thermogravimetric analyser (Thermal Analysers Discovery SDT 650), with a 10 ºC/min heating rate from 50-900 ºC, under 20 ml/min air flow.

Section S2. Investigation of the control catalyst

According to characterization discussed in the main article, nanorod-like morphology OMA (ordered mesopores alumina) catalysts containing different amounts of NiO and Nb_2O_5 could be achieved using the glycol-thermal synthesis technique. However, two key questions remain unanswered. First, what is the main reason for the formation of nanorod morphology? Second, what is the main parameter in controlling the porosity that results in the ordered mesoporous structures in these nanocomposites?

To answer these two questions, a nanocomposite with the elemental composition of NiO = 87.6 wt%, Nb_2O_5 = 6.2 wt% and Al_2O_3 = 6.2 wt% (confirmed by ICP) was synthesised using the glycol-thermal technique. This nanocomposite was characterized using PXRD, N_2-physisorption, TEM and SEM which are shown in **Fig S6** and again a nanorod-like morphology for this material was obtained. This observation clearly shows that the formation of nanorods originated from the synthesis technique. In addition, the nitrogen adsorption-desorption isotherm of this sample shows a type IV isotherm with a H1 type hysteresis loop (**Fig S6b**), indicative of a mesoporous structure. However, the shallow capillary condensation step of this nanocomposite reveals the sample has an irregular mesoporous structure. Therefore, the second question can be answered by stating that the mesoporosity seems to originate

from the glycol-thermal synthesis. However, the presence of alumina appears to be necessary for the synthesis of ordered mesoporous materials via this method.

Section S3. *n*-octane activation under aerobic conditions (full interpretation):

The catalysts were tested in ODH of *n*-octane at different temperatures and the conversions are shown in **Fig S12**. The catalyst containing the highest NiO loading and no niobium additive (NiAl) was found to give the lowest conversion amongst all catalysts at all temperatures (**Fig S12**). According to *in situ* XRD (**Fig S10**) and TP-ROR data (**Fig 3**), the confinement effect negatively influenced the redox properties of this catalyst and may thus compromise the *n*-octane and oxygen conversion in the ODH reaction of *n*-octane using air as an oxidant (**Fig S12**).

The catalyst 2Ni1NbAl was more active than NiAl. Based on TP-ROR and *in situ* XRD data (**Fig 3b** and **Fig S10b**), the confinement effect between NiO and alumina species in a single rod for this catalyst is weaker at temperatures above 400 °C due to changes induced by the redox cycles, which improved the redox properties of this catalyst and enhanced the conversion (**Fig S12**) relative to the other catalysts.

Catalyst 1Ni2NbAl was the most active catalyst at all investigated temperatures (**Fig S12**). This activity was expected, since this catalyst showed a low reduction temperature for NiO species implying a weak interaction between alumina and NiO in this catalyst, which allows redox cycles at relatively low temperatures (**Fig 3c**). However, the conversion was limited at 440 °C by the absence of sufficient oxygen in the reaction stream (**Fig S12b**). Catalyst NbAl also showed moderate activity at all three temperatures. Based on previous reports, on Nb_2O_5, this catalyst cannot follow redox cycles under the chosen reaction conditions, and more specifically the chosen temperatures.[1, 2] Therefore, these conversion values are possibly due to radical [3] and acid-base (**Table 2**) catalysed reactions[4] over this high surface area mesoporous catalyst. The oxygen conversions (**Fig S12b**) match the obtained trend for *n*-octane conversions well.

Fig S13 shows the selectivity to the different products in the ODH of *n*-octane at different temperatures using air as an oxidant. NiAl showed the highest selectivity to octene isomers at all temperatures (**Fig S13a**). The selectivity to octene decreased as the temperature increased, which may imply the conversion of the formed octene to other, secondary, products. The selectivity to aromatics increased at higher temperatures (**Fig S13b**), which suggests that the further dehydrogenation of the formed

octenes and their aromatization requires higher temperatures.[5] The selectivity towards cracked products (**Fig S13c**) has a volcano shape for this catalyst over the three temperatures. This trend suggests that 400 °C is not sufficiently hot to convert the cracked products to CO_x, while 440 °C seems to further crack the short chain products and result in CO_x formation (**Fig S13c and d**).

The selectivity to octene decreased when Nb was introduced, as is shown for 2Ni1NbAl in **Fig S13a**. However, this selectivity remained almost unchanged over 2Ni1NbAl when the temperature was increased from 360 °C to 400 °C, while the conversion increased by almost 8% (**Fig S13a**). The constant selectivity at two different temperatures implies that only the rate of reaction on the same active site increased, while the primary products did not react further due to increase in the reaction temperature. However, the increase of temperature to 440 °C amplifies the activity of the existing sites or changes them towards cracked products, aromatics and CO_x formation that are the products of secondary reactions or deep oxidation of the feed. The same increase in selectivity to aromatics was observed with increasing temperature as was seen for NiAl (**Fig S13b**). Interestingly, increasing the temperature from 360 °C to 400 °C resulted in lower selectivity to cracked products and CO_x for NiAl (**Fig S13c** and **d**). The activation of desired active sites (or nucleophilic oxygen species) for the ODH reaction at this temperature might be the reason for this change, which was different from the observed behaviour for NiAl, but often observed in various ODH systems for medium-chain paraffins.[5, 6] Regardless, the temperature change from 400 °C to 440 °C resulted in cracking and combustion of the formed alkenes, as was observed in the case of NiAl.

1Ni2NbAl gave the lowest selectivity to octenes at all temperatures. A large drop in selectivity to octenes can be seen in **Fig S13a** when the temperature was increased from 360 °C to 400 °C. This result was expected, since the conversion between these temperatures showed a large increase and a sharp reduction at approximately this temperature was observed in the *in situ* XRD and H_2-TPR analyses for this catalyst (**Fig S10c, 3c**). However, the selectivity did not change significantly above 400 °C, suggesting the occurrence of only one reduction step in this catalyst, as indeed is seen in the *in situ* XRD and TP-ROR data (**Fig S10c and 3c**). Generally, the selectivity to aromatics increased with increasing temperature, as was observed for the two other nickel containing catalysts (**Fig S13b**). The

selectivity to cracked products and CO_x increased as the temperature was increased from 360 °C to 400 °C and stayed almost the same between 400 °C and 440 °C (**Fig S13c** and **d**). In addition, the increase in conversion and the general maintenance of selectivity toward different products between 400 °C to 440 °C suggests that temperature only affects the reaction rate without modifying the active sites for different reactions involved in this catalytic system.

NbAl showed a consistent decrease in selectivity to octenes as the temperature was increased (**Fig S13a**), with the opposite trend was observed for CO_x selectivity (**Fig S13d**). Selectivity to aromatics increased initially, when the temperature was increased from 360 °C to 400 °C, but decreased when the temperature was increased further to 440 °C (**Fig S13b**). Almost the same trend was observed for cracked products (**Fig S13c**). According to NH_3-TPD data (**Table 2**) and literature on Nb, the addition of this element generally increases the density of acidic sites, which seem to strongly contribute to cracking of the formed alkenes, and, in this case, even the more stable products like aromatics.[7] Based on literature, NbAl is not capable of redox behaviour under these conditions, acid catalysed and thermal reactions seem to dominate in this case.[1, 2, 4]

The cracking of ethylbenzene and styrene normally results in the formation of benzene, which is shown in **Table S2**. Generally, the selectivity towards benzene (**Table S2**) matches well with the observed trend of total acidity over these catalysts (**Table 2**). In addition, selectivities to CO and CO_2 are shown in **Table S2**. CO is known to originate from cracking and oxygen insertion of the formed hydrocarbons during reactions (**Table S2**).[8, 9]

The effect of changing the concentration of oxygen in the reaction stream on catalytic performance is shown in **Fig S14**. The amount of O_2 in the reaction has a direct correlation with the conversion of *n*-octane. NiAl showed the best selectivity to octene isomers at the different C:O ratios, while a lower conversion was observed over this catalyst in comparison to other catalysts (**Fig S14**). 2Ni1NbAl and NbAl showed almost the same trend of deactivation and improved selectivity when the reaction proceeded at high C:O ratios (**Fig S14**). However, a faster drop in conversion (upon changing C:O ratios) was observed over 1Ni2NbAl than over the other catalysts when the concentration of oxygen in

the reaction stream was lowered. Also, the positive impact of this change in selectivity to octene isomers and CO_x was more significant than over the other catalysts. The introduction of a smaller quantity of oxidant seems to slow the reaction by limiting the formation of undesired electrophilic oxygen species that leads to CO_x formation. On the other hand, the coking of undesired catalytic sites (like acidic sites) under anaerobic conditions seems also to selectively lower the CO_x formation and enhance the selectivity to the desired/primary ODH reactions products. The positive impact of coking also is shown in other catalytic applications.[8, 10-12] To see the effect of the alkane chain length in the ODH reaction, propane was tested for this reaction.

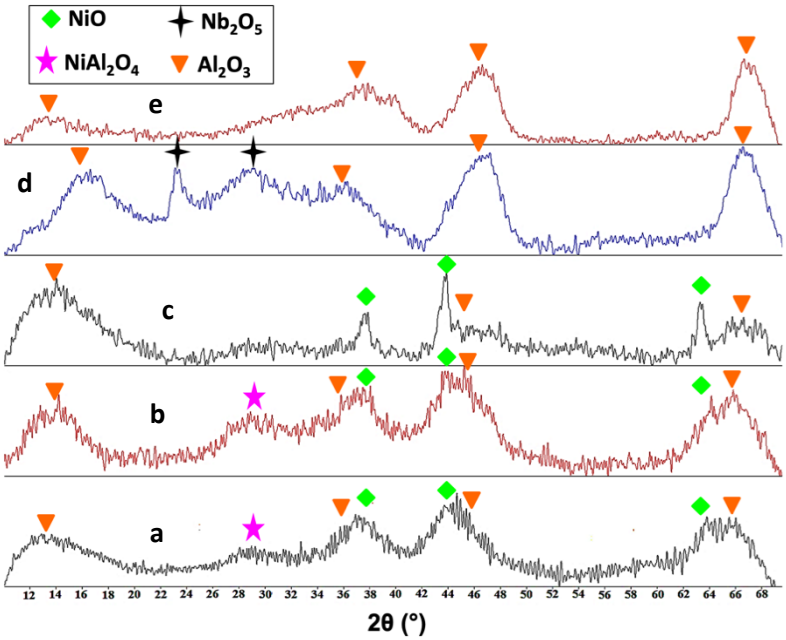

Fig S1. PXRD scans of $Ni_{(3-x)}Nb_{(x)}Al$ (X = 3, 2, 1, 0). a) NiAl, b) 2Ni1NbAl, c) 1Ni2NbAl and d) NbAl, e) Al_2O_3 prepared using the glycol-thermal technique.

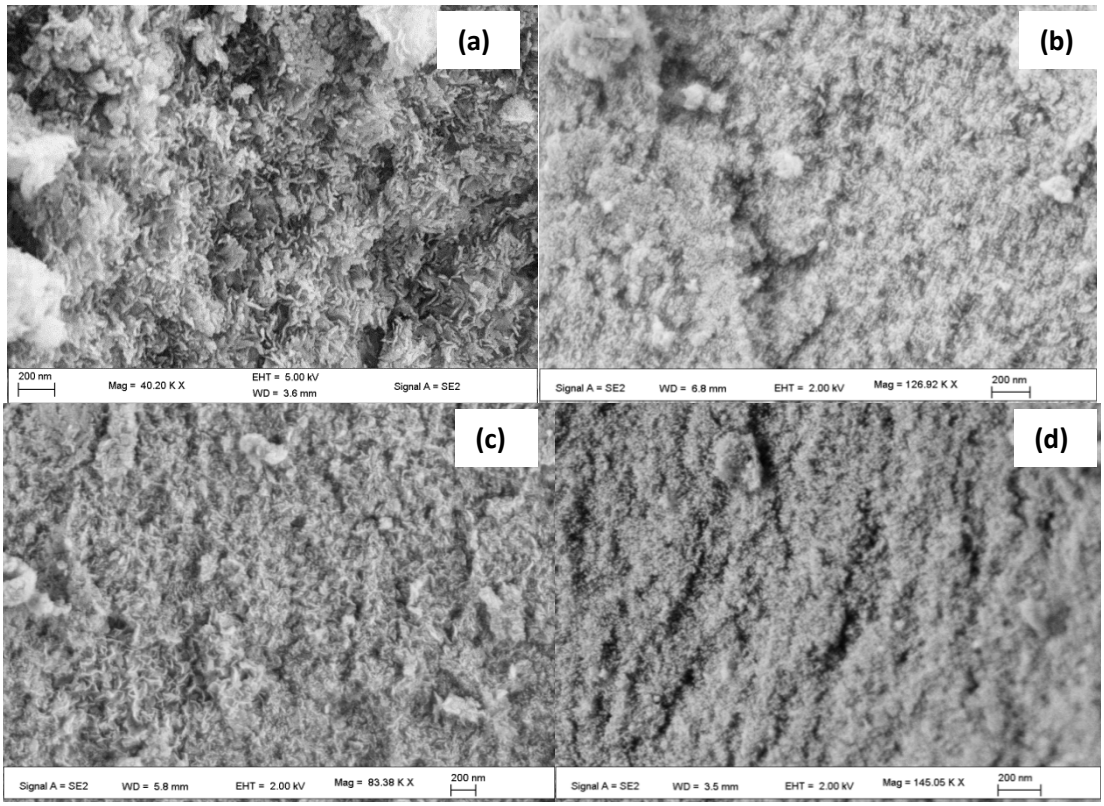

Fig S2. SEM images of all catalysts. a) NiAl, b) 2Ni1NbAl, c) 1Ni2NbAl and d) NbAl.

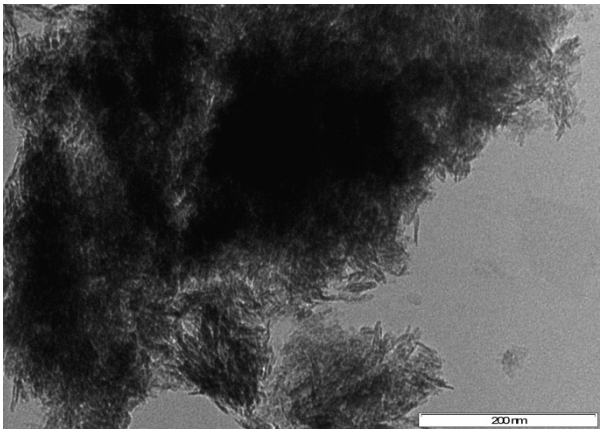

Fig S3. TEM image of Al_2O_3 synthesised using the glycol-thermal technique.

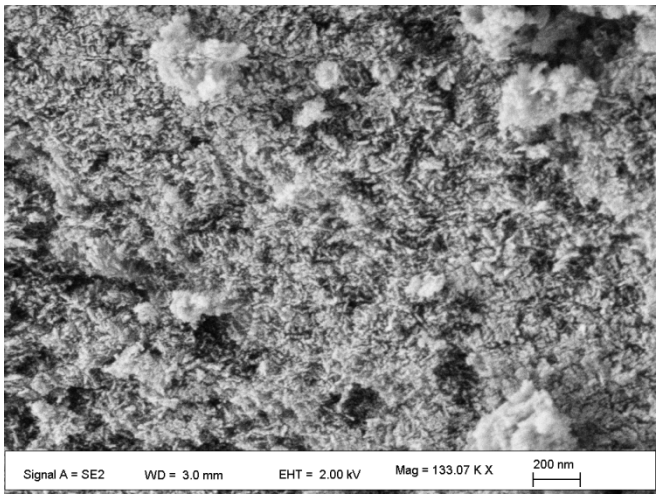

Fig S4. SEM image of Al_2O_3 synthesised using the glycol-thermal technique.

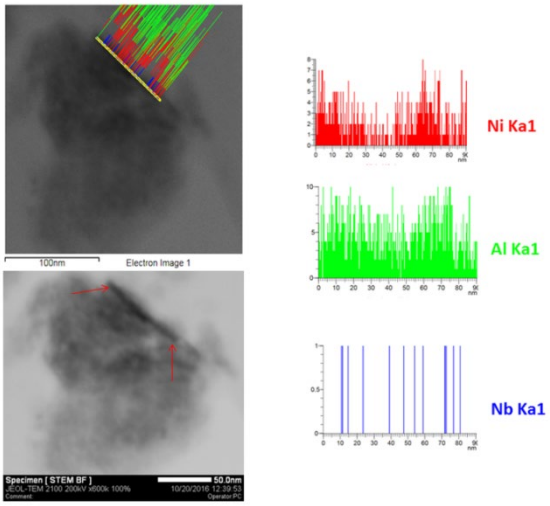

Fig S5. Line scan of a single nanorod of 2Ni1NbAl using HR-TEM in STEM mode (bright field). (Smaller nanorods are present, but could not be viewed due to the lower resolution obtained when the scanning mode of the HR-TEM was used).

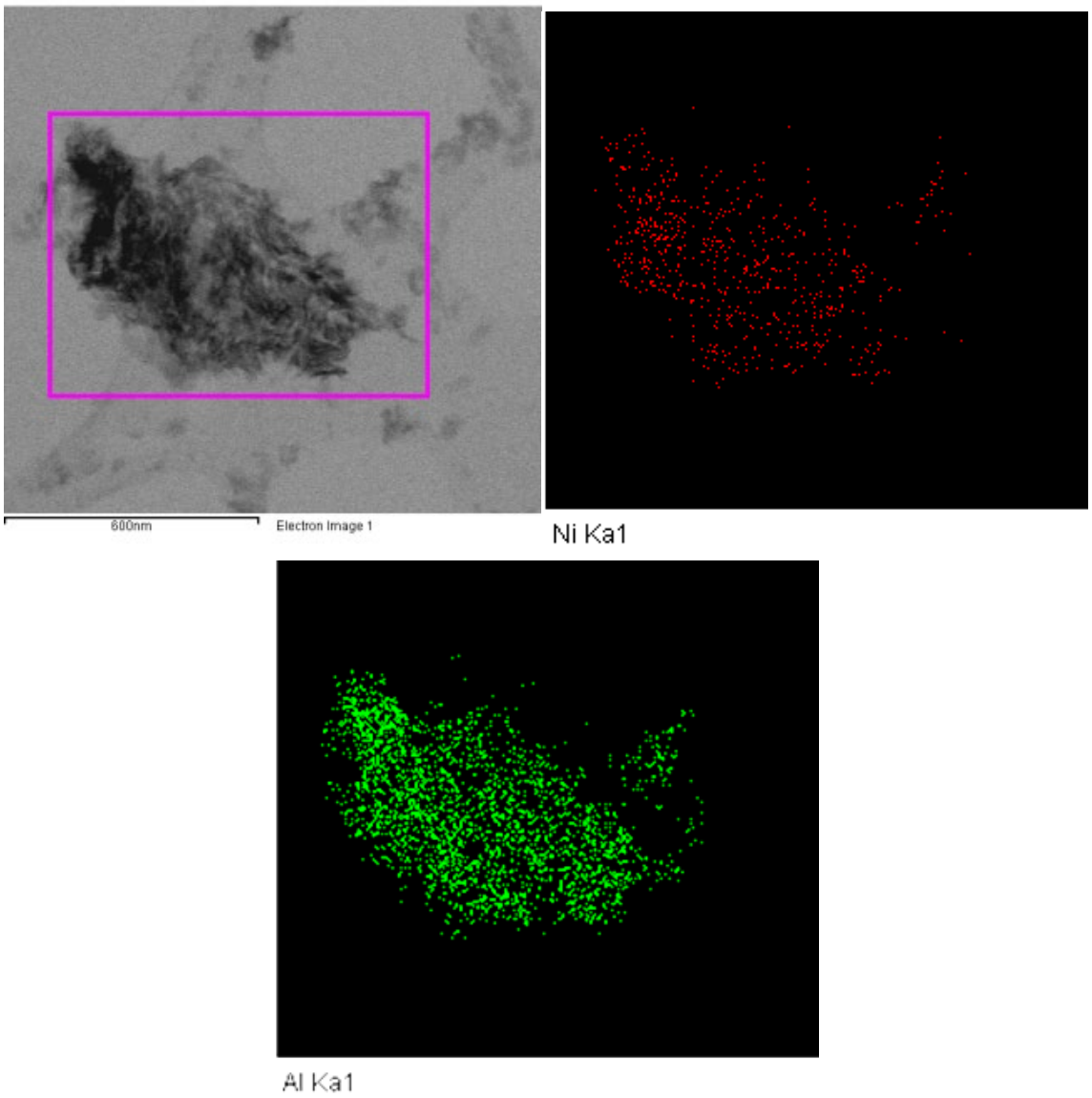

Fig S6. Elemental mapping of NiAl, using HR-TEM (bright field in STEM mode).

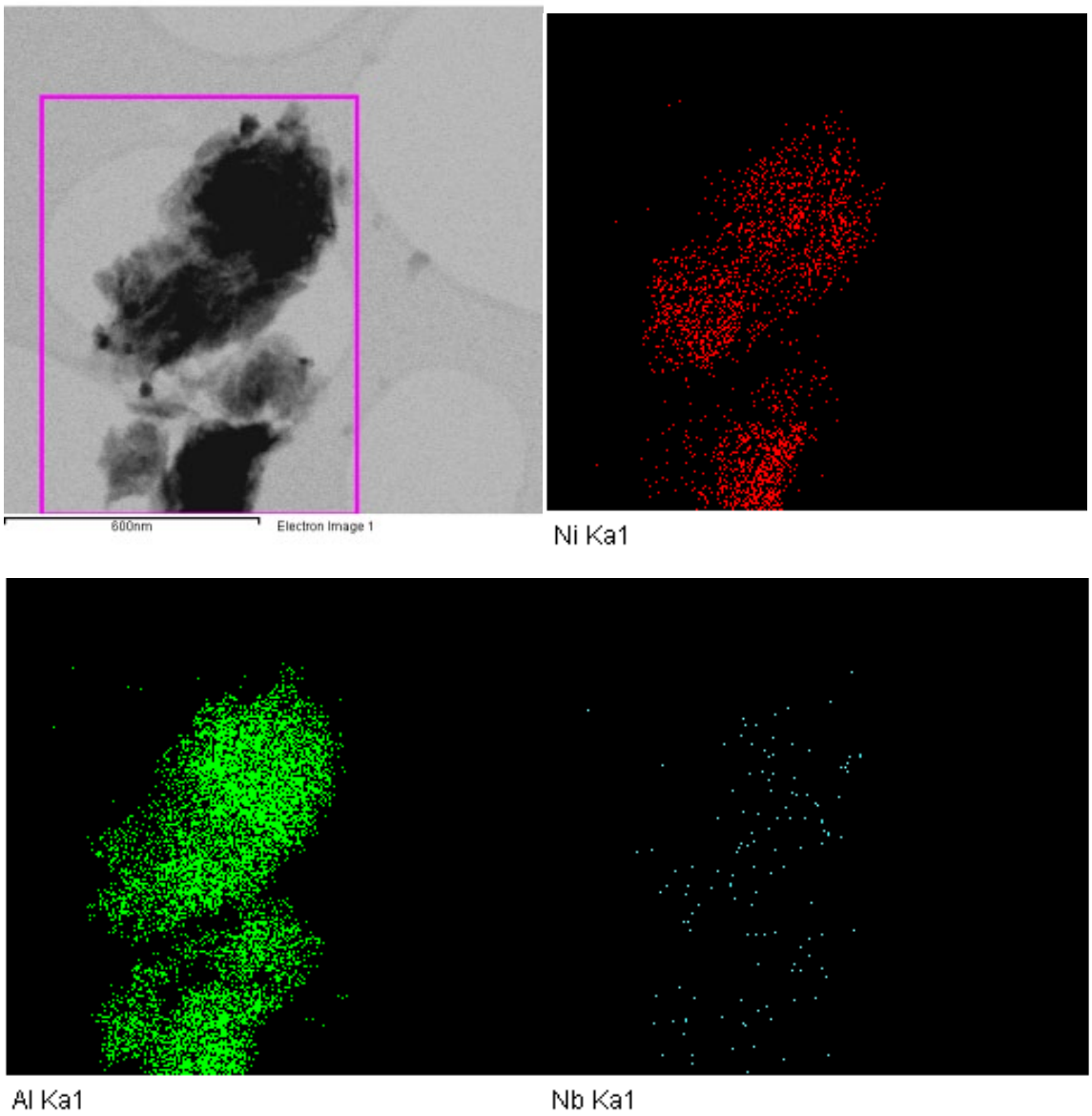

Fig S7. Elemental mapping of 2Ni1NbAl, using HR-TEM (bright field in STEM mode).

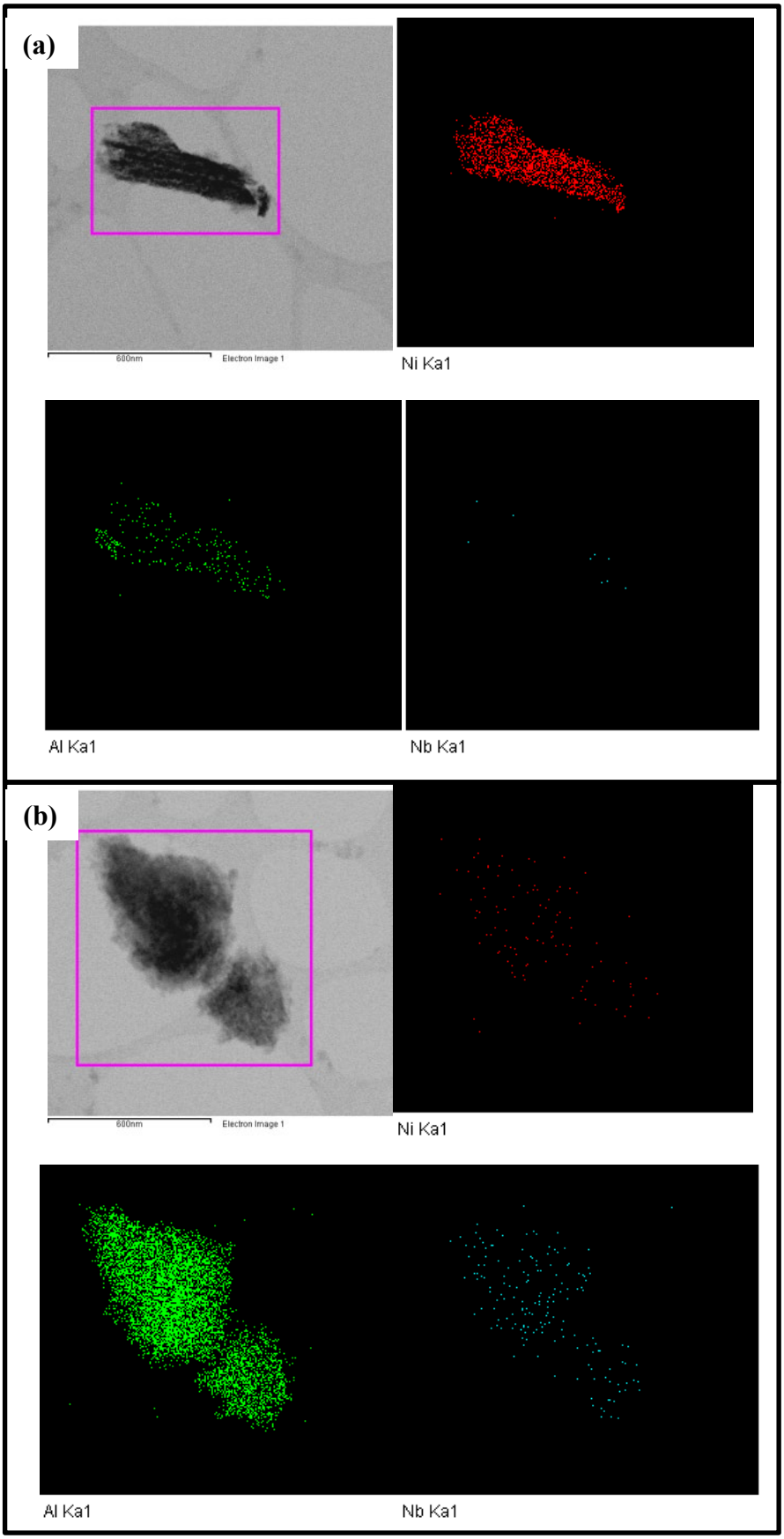

Fig S8. Elemental mapping of 1Ni2NbAl, (a) site with high nickel content, (b) site with low nickel content, using HR-TEM (bright field in STEM mode).

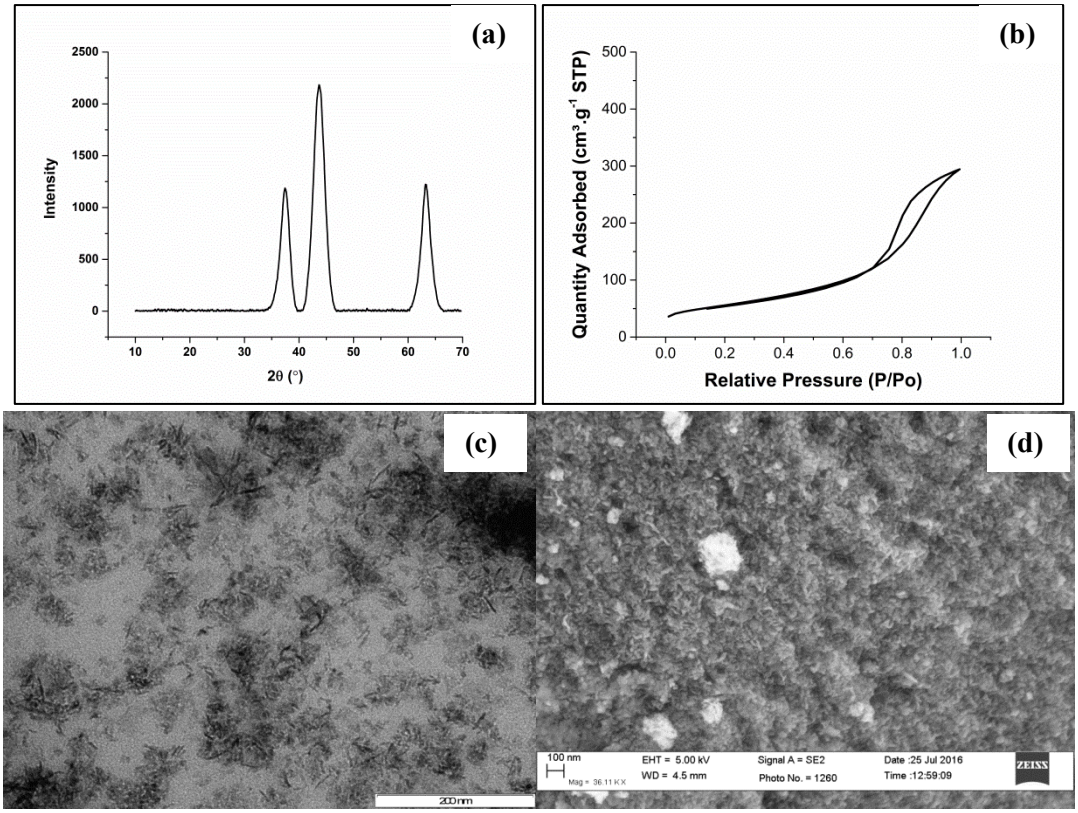

Fig S9. The basic characterisations of the synthesised control catalyst with the composition of NiO = 87.6 wt.%, Nb_2O_5 = 6.2 wt.% and Al_2O_3 = 6.2 wt.%. (a) PXRD, (b) N_2 adsorption-desorption isotherm, (c) TEM image and (d) SEM image.

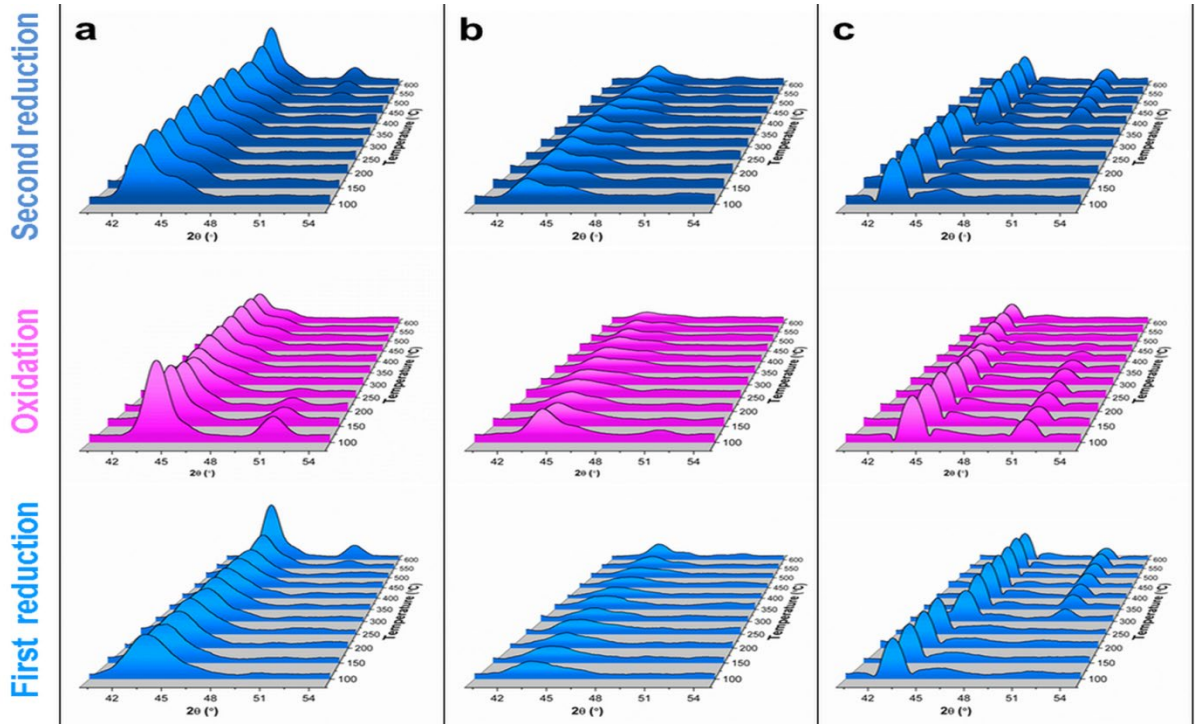

Fig S10. *In situ* XRD analysis of nickel containing catalysts. a) NiAl, b) 2Ni1NbAl and c) 1Ni2NbAl. The catalysts were reduced in the first step, then oxidised, followed by the second reduction. Temperature range = 100 - 600 °C. The peak representing NiO has a 2θ value of 44°, while metallic Ni has two peaks with 2θ values of 46° and 53°.

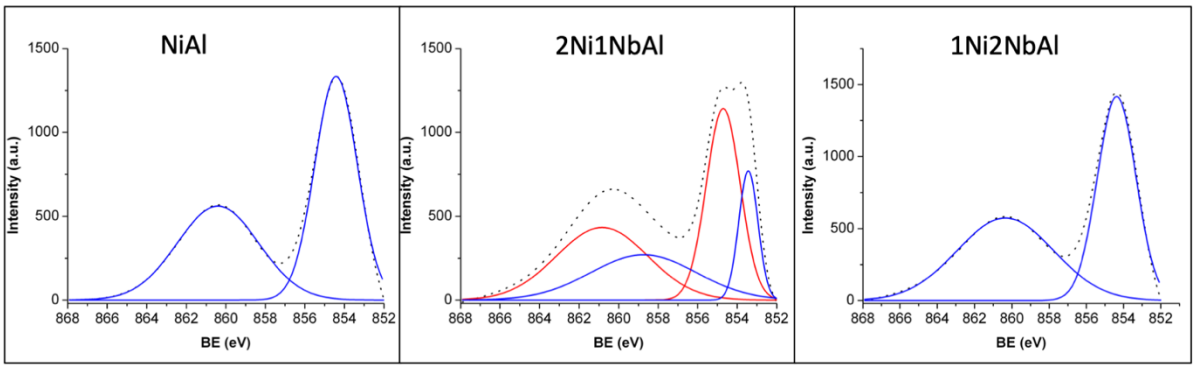

Fig S11. Deconvoluted XPS of nickel containing catalysts Ni 2p3/2 orbital.

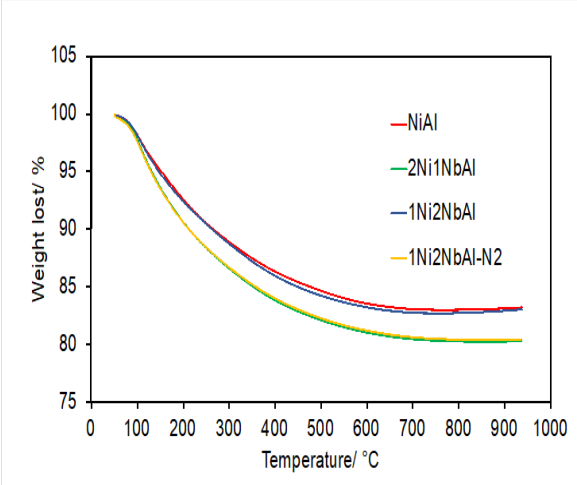

Fig S12. TGA of fresh nickel containing catalysts under flow of air except for 2Ni1NbAl-N2 (yellow curve) where the TGA was obtained under nitrogen atmosphere.

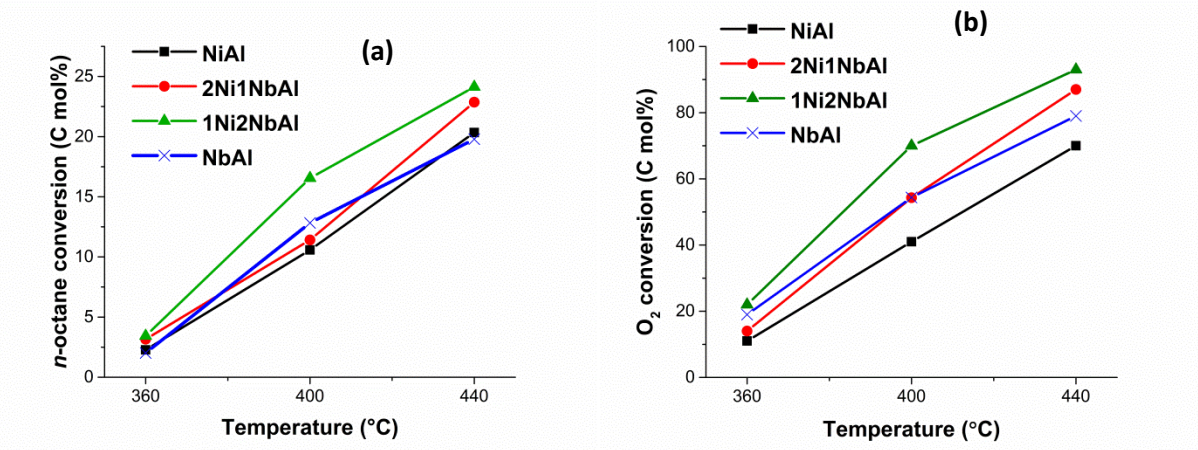

Fig S13. a) *n*-octane conversion and b) oxygen conversion in ODH of *n*-octane over all catalysts. Reaction conditions: C:O = 8:4, GHSV = 16 000 h^{-1} and concentration of *n*-octane in the feed = 7%.

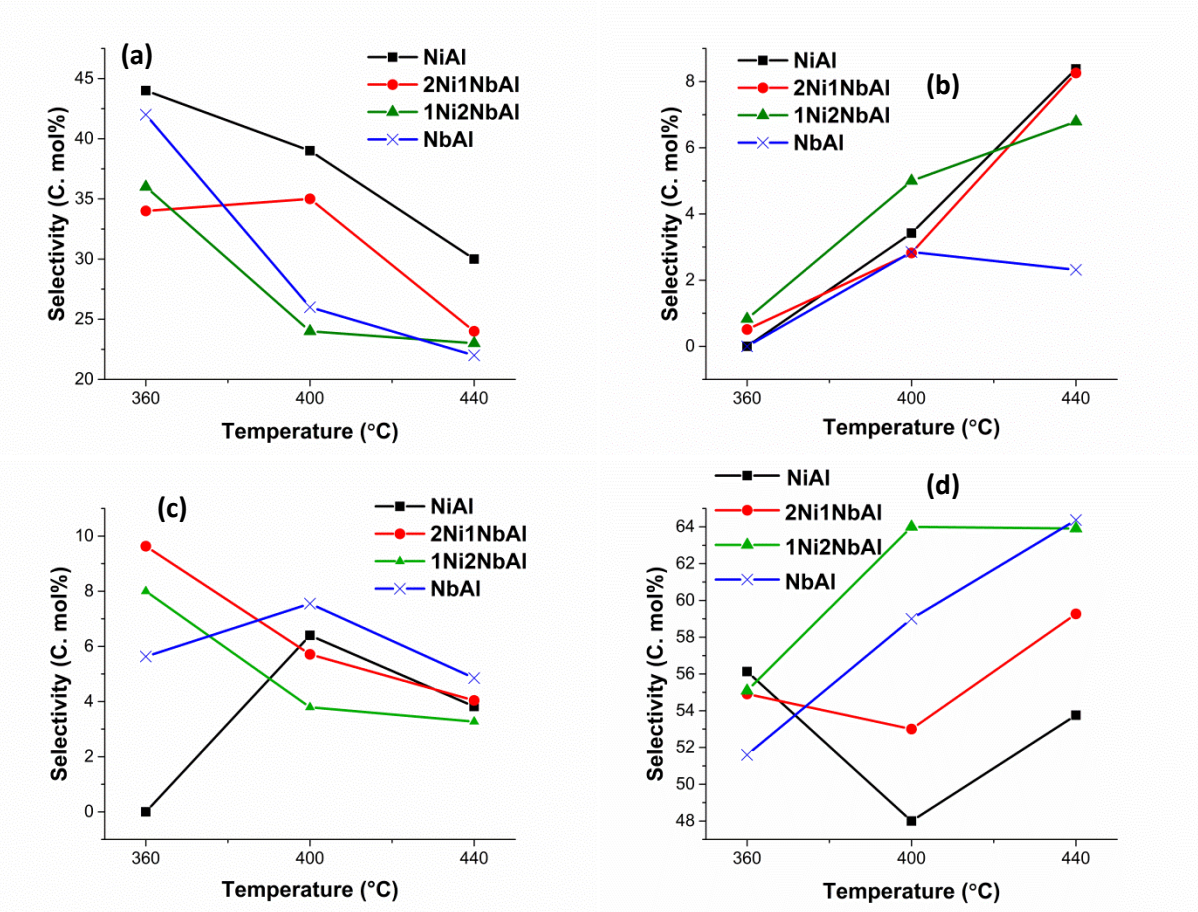

Fig S14. a) Selectivity to octene isomers, b) selectivity to different aromatics, c) selectivity to cracked products and d) selectivity to CO_x in ODH of *n*-octane over all catalysts. Reaction conditions: C:O = 8:4, GHSV = 16 000 h^{-1} and concentration of *n*-octane in the feed = 7%.

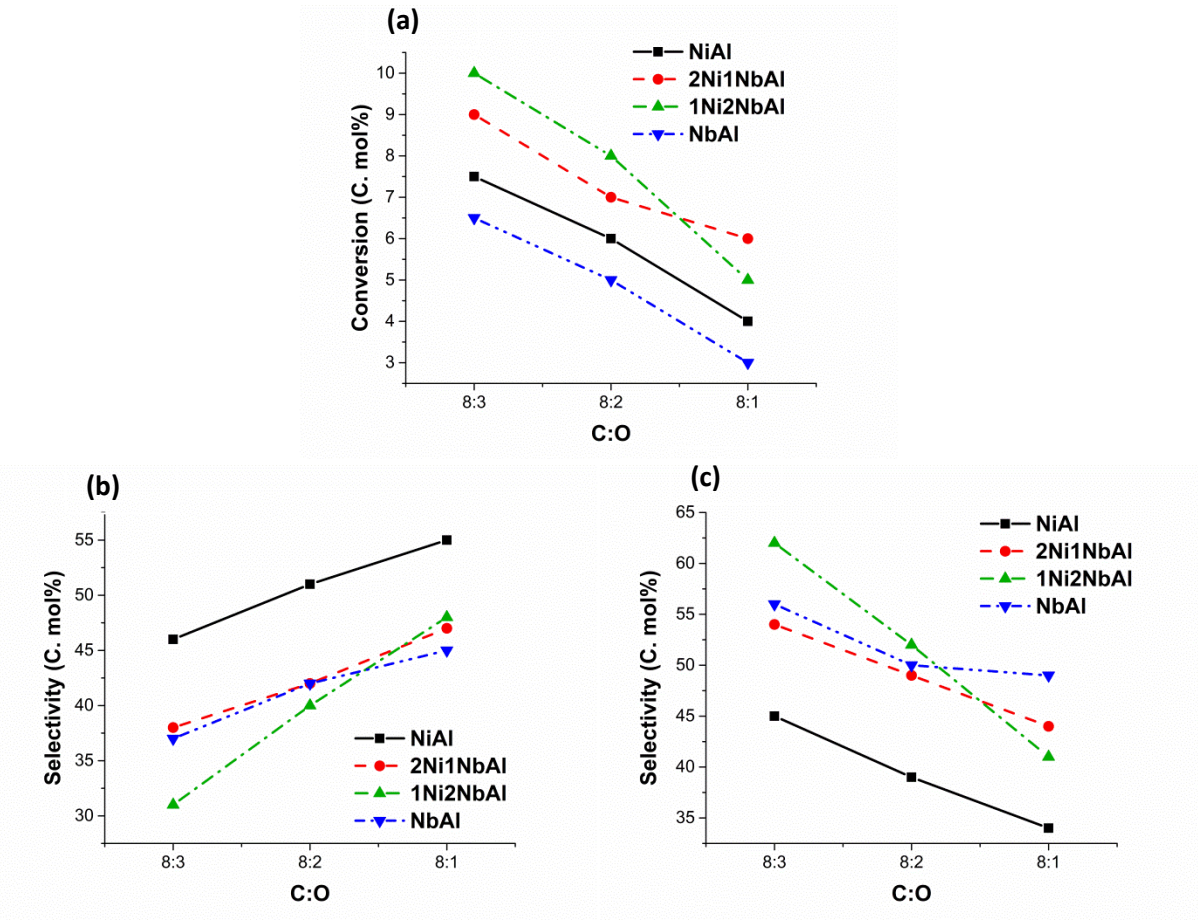

Fig S15. The effect of C:O ratio variation on oxidative conversion of *n*-octane over all catalysts. a) *n*-octane conversion, b) selectivity to octene isomers and c) selectivity to CO_x.

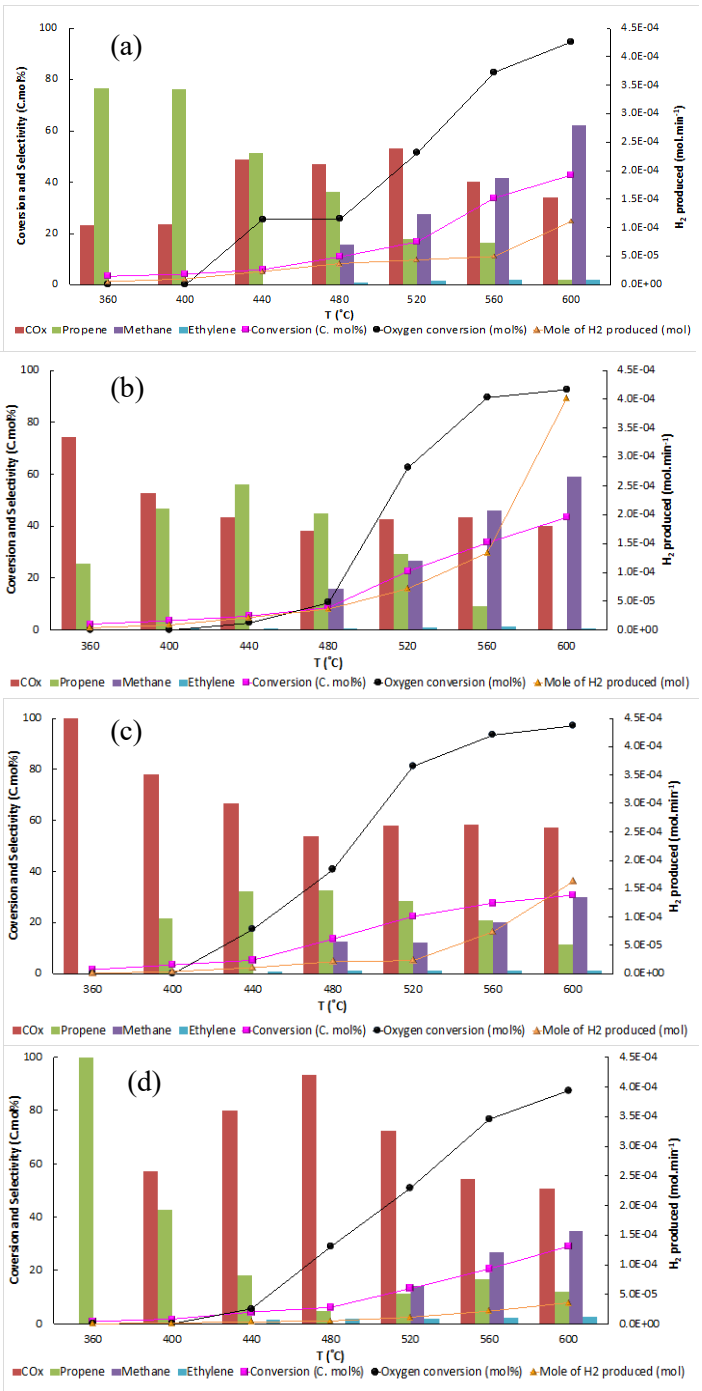

Fig S16. The oxidative dehydrogenation of propane using air as an oxidant (a) NiAl, (b) 2Ni1NbAl, (c) 1Ni2NbAl and (d) NbAl. Reaction conditions: C:O = 3:1.5, GHSV = 16 000 h^{-1} and concentration of propane in the feed = 19%.

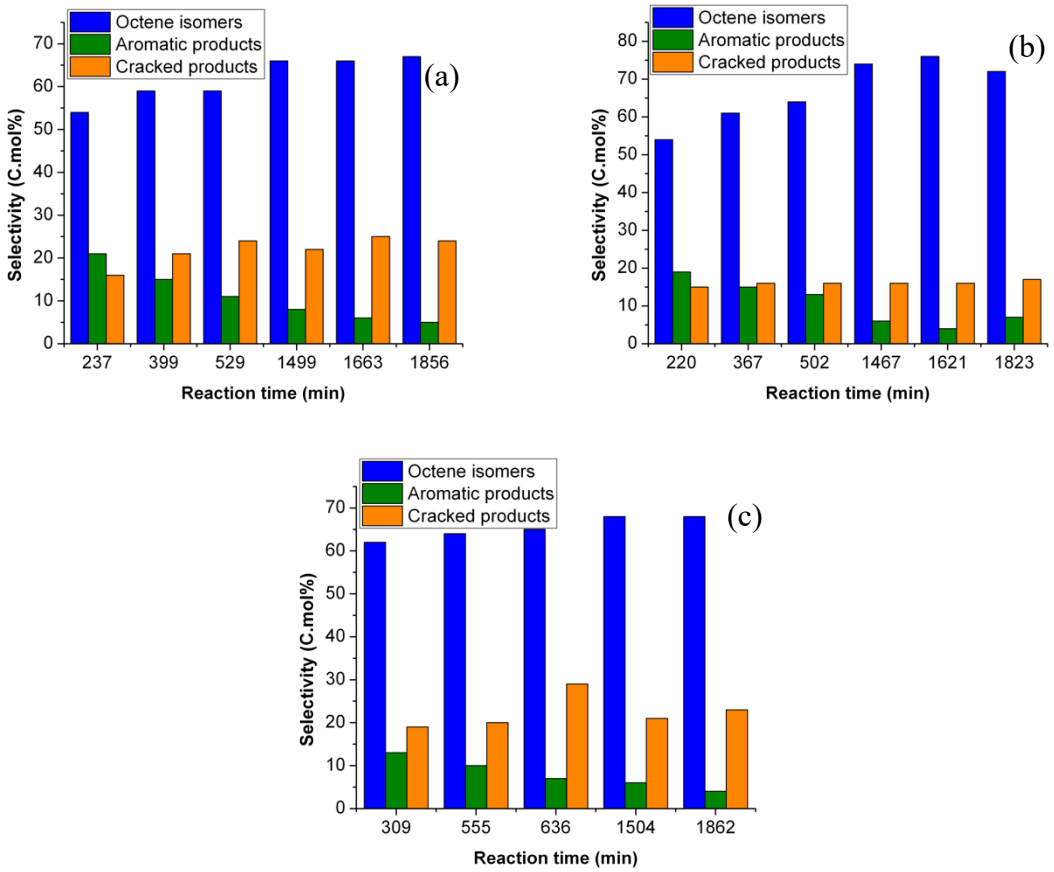

Fig S17. Selectivity to different products during the DH of *n*-octane. (a) NiAl, (b) 2Ni1NbAl and (c) 1Ni2NbAl. Reaction conditions: Temperature = 550 °C, GHSV = 13 000 h^{-1} and concentration of *n*-octane in the feed = 12%.

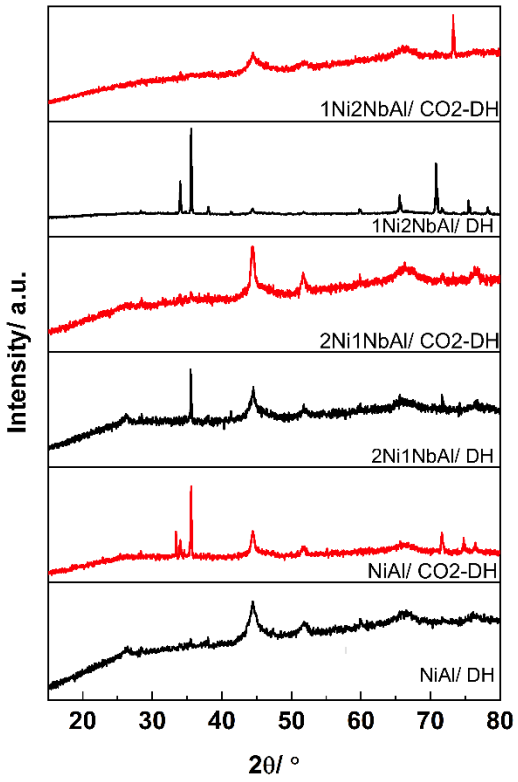

Fig S18. XRD of the used catalysts obtained after DH and CO_2-DH.

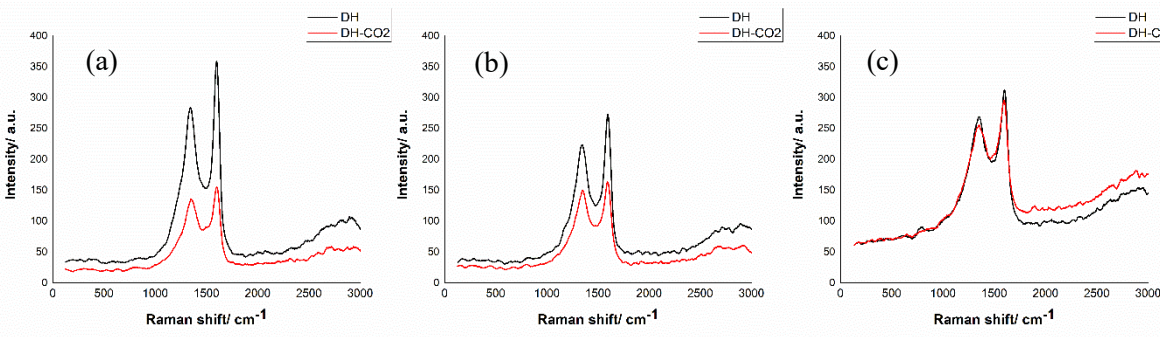

Fig S19. Raman spectra of the used catalysts obtained after DH and CO_2-DH catalytic runs. (a) NiAl, (b) 2Ni1NbAl and (c) 1Ni2NbAl.

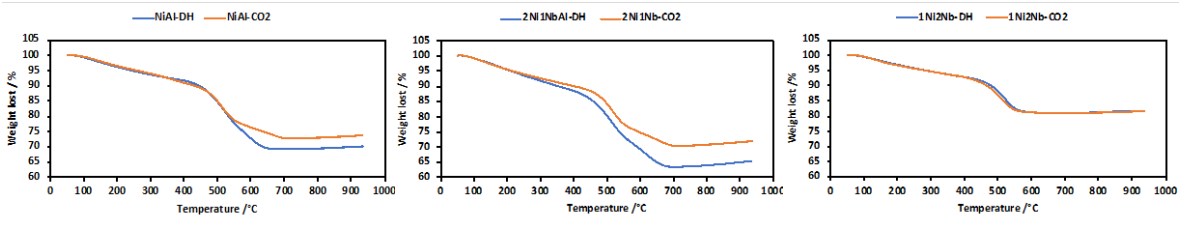

Fig S20. TGA of the used catalysts obtained after DH and CO_2-DH catalytic runs.

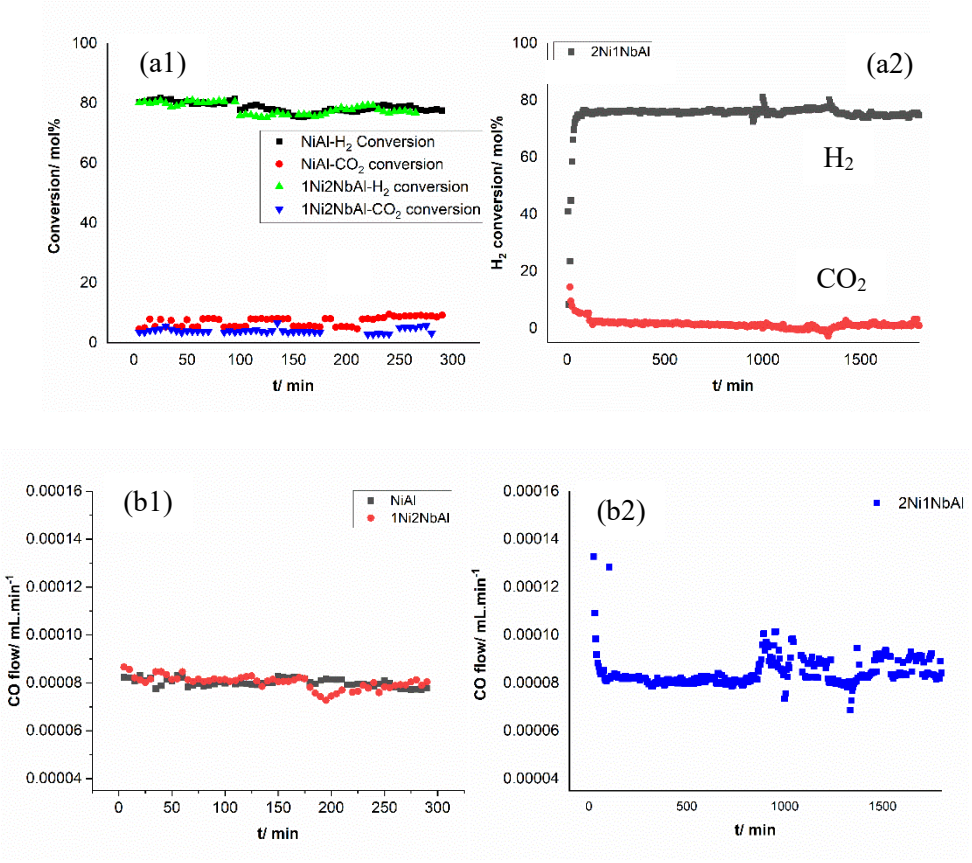

Fig S21. (a1-2) H_2 and CO_2 conversions. (b1-2) CO flow.

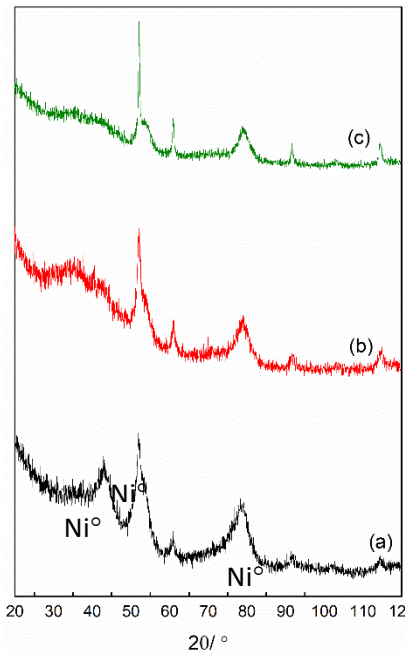

Fig S22. XRD of the used catalysts obtained after RWGS reaction using CO_2. (a) NiAl, (b) 2Ni1NbAl and (c) 1Ni2NbAl. (The used catalysts were passivated using N_2 after the reaction)

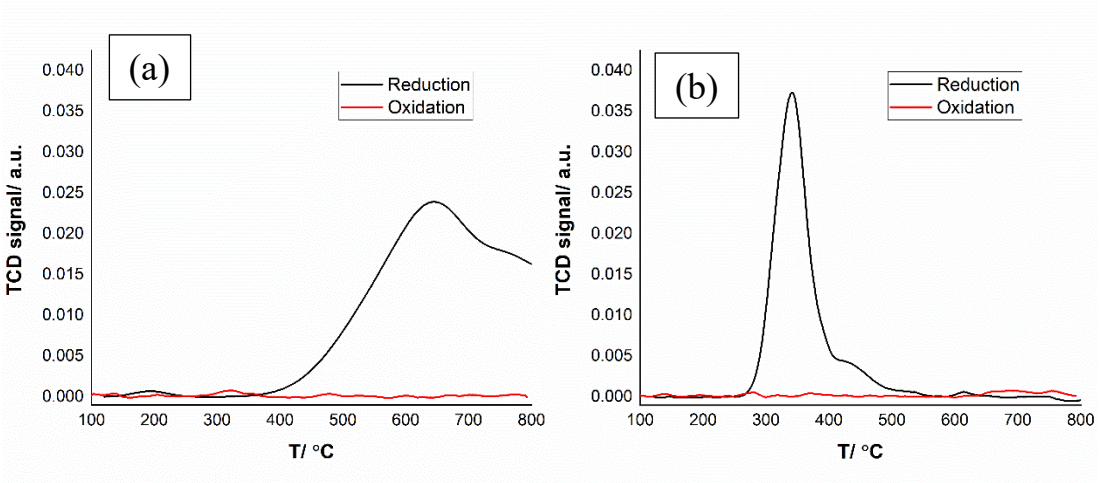

Fig S23. TP-RO using H_2 as a reductant and CO_2 as an oxidant (a) 2Ni1NbAl and (b) 1Ni2NbAl.

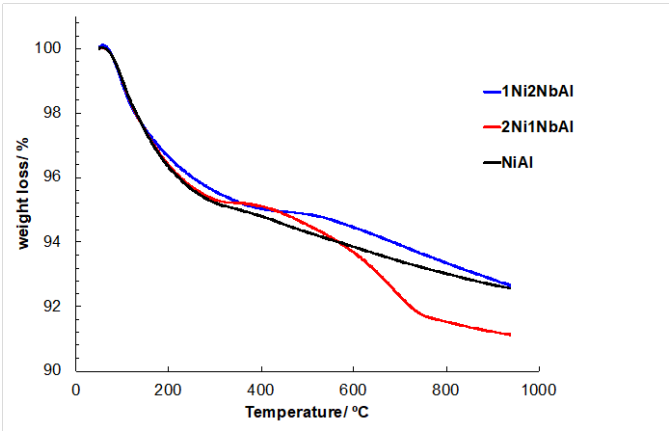

Fig S24. TGA of the used catalysts obtained after RWGS testing.

Table S2. Selectivity to CO_2, CO and benzene over all catalysts.

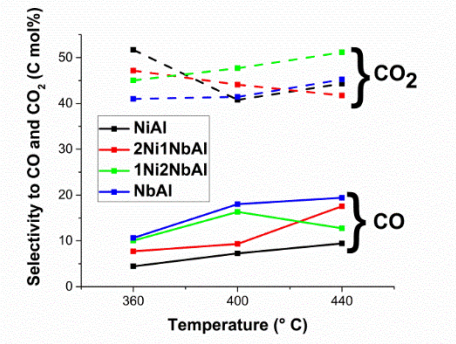

Catalyst	Selectivity to benzene (C mol%)		
	360 °C	400 °C	440 °C
NiAl	0	1	2
2Ni1NbAl	0	1	3
1Ni2NbAl	0	2	2
NbAl	0	4	6

References

1. E. Heracleous and A. A. Lemonidou, *J. Catal.*, 2006, **237**, 162-174.
2. Z. Skoufa, E. Heracleous and A. A. Lemonidou, *Catal. Today*, 2012, **192**, 169-176.
3. S. Furukawa, T. Shishido, K. Teramura and T. Tanaka, *J. Phys. Chem. C*, 2011, **115**, 19320-19327.
4. K. Nakajima, Y. Baba, R. Noma, M. Kitano, J. N. Kondo, S. Hayashi and M. Hara, *J. Am. Chem. Soc.*, 2011, **133**, 4224-4227.
5. E. A. Elkhalifa and H. B. Friedrich, *Appl. Catal., A*, 2010, **373**, 122-131.
6. S. Pradhan, J. K. Bartley, D. Bethell, A. F. Carley, M. Conte, S. Golunski, M. P. House, R. L. Jenkins, R. Lloyd and G. J. Hutchings, *Nat. Chem.*, 2012, **4**, 134-139.
7. C. A. Gärtner, A. C. van Veen and J. A. Lercher, *ChemCatChem*, 2013, **5**, 3196-3217.

8. M. D. Farahani, V. D. B. C. Dasireddy and H. B. Friedrich, *ChemCatChem*, 2018, **10**, 2059-2069.

9. M. I. Fadlalla, M. D. Farahani and H. B. Friedrich, *Mol. Catal.*, 2018, **461**, 86-96.

10. D. Teschner, E. Vass, M. Hävecker, S. Zafeiratos, P. Schnörch, H. Sauer, A. Knop-Gericke, R. Schlögl, M. Chamam, A. Wootsch, A. S. Canning, J. J. Gamman, S. D. Jackson, J. McGregor and L. F. Gladden, *J. Catal.*, 2006, **242**, 26-37.

11. J. McGregor, Z. Huang, E. P. J. Parrott, J. A. Zeitler, K. L. Nguyen, J. M. Rawson, A. Carley, T. W. Hansen, J.-P. Tessonnier, D. S. Su, D. Teschner, E. M. Vass, A. Knop-Gericke, R. Schlögl and L. F. Gladden, *J. Catal.*, 2010, **269**, 329-339.

12. S. Gomez Sanz, L. McMillan, J. McGregor, J. A. Zeitler, N. Al-Yassir, S. Al-Khattaf and L. F. Gladden, *Catal. Sci. Tech.*, 2015, **5**, 3782-3797.